Research Article Vol. 5, No. 5 / May 2018 / Optica 644

Electrical control of nonlinear quantum optics in a nano-photonic waveguide

Dominic Hallett,[1,†] Andrew P. Foster,[1,†,*] David L. Hurst,[1] Ben Royall,[1] Pieter Kok,[1] Edmund Clarke,[2] Igor E. Itskevich,[3] A. Mark Fox,[1] Maurice S. Skolnick,[1] and Luke R. Wilson[1]

[1]Department of Physics and Astronomy, University of Sheffield, Sheffield S3 7RH, UK
[2]Department of Electronic and Electrical Engineering, University of Sheffield, Sheffield S1 3JD, UK
[3]School of Engineering and Computer Science, University of Hull, Hull HU6 7RX, UK
*Corresponding author: andrew.foster@sheffield.ac.uk

Received 24 January 2018; revised 30 March 2018; accepted 6 April 2018 (Doc. ID 319959); published 16 May 2018

Quantum photonics is a rapidly developing platform for future quantum network applications. Waveguide-based architectures, in which embedded quantum emitters act as both nonlinear elements to mediate photon–photon interactions and as highly coherent single-photon sources, offer a highly promising route to realize such networks. A key requirement for the scale-up of the waveguide architecture is local control and tunability of individual quantum emitters. Here, we demonstrate electrical control, tuning, and switching of the nonlinear photon–photon interaction arising due to a quantum dot embedded in a single-mode nano-photonic waveguide. A power-dependent waveguide transmission extinction as large as $40 \pm 2\%$ is observed on resonance. Photon statistics measurements show clear, voltage-controlled bunching of the transmitted light and antibunching of the reflected light, demonstrating the single-photon, quantum character of the nonlinearity. Importantly, the same architecture is also shown to act as a source of highly coherent, electrically tunable single photons. Overall, the platform presented addresses the essential requirements for the implementation of photonic gates for scalable nano-photonic-based quantum information processing.

OCIS codes: (230.5590) Quantum-well, -wire and -dot devices; (270.0270) Quantum optics; (130.5990) Semiconductors; (350.4238) Nanophotonics and photonic crystals.
https://doi.org/10.1364/OPTICA.5.000644

1. INTRODUCTION

Integrated quantum photonic systems, in which quantum states of light are generated, manipulated, and detected on-chip, are rapidly evolving as a scalable approach for quantum information science and technologies. Efficient generation of indistinguishable single photons and control of photon–photon interactions are essential requirements for the practical implementation of integrated quantum photonics in quantum optical networks and photonic quantum computing. Integrated architectures in which embedded, waveguide-coupled quantum emitters can act as photon sources and also provide the saturable nonlinearity to mediate photon–photon interactions provide a particularly compact and scalable solution. Further key advantages of this approach include efficient coupling of the quantum emitter to a single optical mode [1] and wide bandwidth waveguide operation [2], with recent work demonstrating the significant potential of this approach using InGaAs quantum dots (QDs) [3,4] and color centers in diamond [5,6]. The deterministic nature of the nonlinearity can be exploited in future photonic gates such as the controlled-phase [7–9] and controlled-NOT [10] gates, the building blocks for quantum computation using photons [11,12]. Exotic states of light, such as photon–photon bound states [13], may be derived from the nonlinear interaction. A single-photon nonlinearity could also find use in classical applications such as optical routing [14] and single photon transistors [15].

Further advances in these directions require local electrical control of the waveguide-coupled quantum emitters, providing static and dynamic tuning to address challenges including emitter spectral mismatch [16] and the need for fast switching [12]. For semiconductor QD-based systems, embedding QDs in bulk Schottky or *p-i-n* structures allows for charge state selection [17,18] and fast energy tuning of embedded QDs [19,20] via the DC Stark effect, as well as reducing charge noise and increasing single-photon indistinguishability [21]. Semiconductor diodes are also compatible with the generation of transform-limited single photons [22]. The challenge is to transfer similar approaches to waveguide-based integrated photonic systems. One of the key drivers here is that static electrical tuning provides a route to bringing multiple QDs into resonance, a critical step in advancing current technology beyond one and few-emitter

proof-of-concept devices. On the other hand, dynamic electrical control addresses the requirement of quantum information processing for high clock speeds to limit the effects of quantum bit dephasing.

In this work, we demonstrate electrical control of resonant photon scattering from QDs in an integrated quantum photonic device, providing both spectrally tunable waveguide-coupled single photons and a switchable nonlinear response at the single-photon level. Electrically tunable and switchable waveguide-coupled resonance fluorescence (RF) is measured from both neutral and charged states of the same QD. In waveguide transmission measurements, strong extinction of a weak coherent laser is observed as it is tuned into resonance with the QD. Bunching of the transmitted laser field is accompanied by antibunching of its reflected counterpart, demonstrating the quantum nonlinear nature of the photon–emitter interaction.

2. RESULTS

A. Nano-Photonic Device Design and Characterization

A scanning electron microscope image of our nano-photonic device is shown in Fig. 1(a). A single-mode photonic crystal waveguide (PhCWG) in the center is coupled at either end to nanobeam waveguides that are individually terminated with Bragg grating couplers (BGCs) for vertical in- and out-coupling of light. All structures are defined within a 170 nm thick *p-i-n* GaAs membrane grown on a 1 μm thick AlGaAs sacrificial layer by molecular beam epitaxy [Fig. 1(b)]. The AlGaAs layer was removed using hydrofluoric acid wet-etching to release the GaAs membrane and maximize optical confinement within the waveguides. A layer of self-assembled InGaAs QDs emitting between 880 nm and 940 nm was grown in the middle of the GaAs membrane. Electrical contacts fabricated on the *p* and *n* layers of the membrane enabled Stark-tuning of the QD energy states.

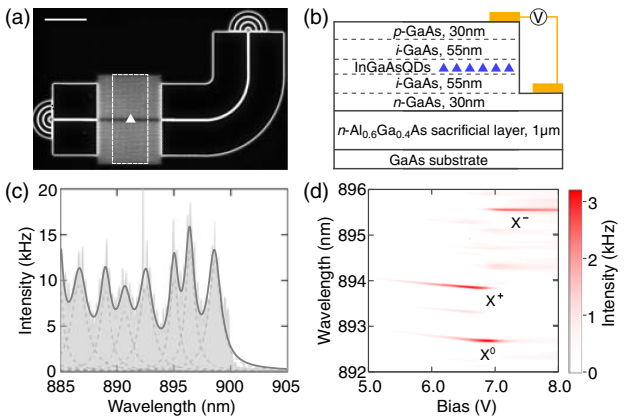

Fig. 1. Characterization of the nano-photonic device. (a) Scanning electron microscope image of the device. The white dashed box encloses the slow light section of the PhCWG. The triangle shows the approximate location of the studied QD. Scale bar 5 μm. (b) Diode structure schematic. Electrical contacts are made to the *p*- and *n*-GaAs layers. (c) High power photoluminescence spectrum at a bias of 8 V showing emission from an ensemble of QDs in the photonic crystal waveguide (light gray shaded region). The waveguide band edge is seen at ∼900 nm. Fabry–Perot oscillations are observed due to reflection from the BGCs. The peaks are fit with multiple Lorentzian curves (dashed lines) with their sum given by the dark gray line. (d) Photoluminescence intensity versus wavelength and bias for non-resonant excitation in the center of the photonic crystal waveguide and collection from one BGC.

The PhCWG was fabricated by omitting one row of holes from a two-dimensional photonic crystal. The central region of the PhCWG was designed with a photonic band edge at ∼900 nm (see sections S1 and S2 of Supplement 1 for more details regarding the PhCWG design). QDs emitting near the band edge experience a Purcell enhancement due to the slow light effect [23] and couple more strongly to the single-waveguide mode [24]. The BGCs have a characteristic linear optical polarization perpendicular to the input waveguide. A 90 deg in-plane bend of one nanobeam waveguide ensured that the two BGCs were orthogonally polarized and thus enabled efficient laser rejection during resonant transmission measurements [3].

The spectral location of the PhCWG band edge was identified using high-power non-resonant photoluminescence (PL) spectroscopy. The QD ensemble within the PhCWG was excited from above and the resulting PL collected from one BGC. Figure 1(c) shows the resulting PL spectrum on excitation of the QD ensemble at 808 nm with a power of 11 μW. The band edge of the waveguide is clearly visible, with a cutoff in transmission at ∼900 nm. The PL spectrum is modulated by Fabry–Perot modes, which are attributed to weak reflection from the BGCs.

On lowering the excitation power to 1.3 μW, PL from individual QDs is observed. Figure 1(d) shows the PL intensity as a function of *p-i-n* junction bias (note that the large biases used in this work arise from series resistance in the contacts and have no noticeable effect on the optical properties of the device). Three bright spectral lines are observed at 893 nm, 894 nm, and 895.5 nm, labeled X^0, X^+, and X^-, respectively [25]. The variation in intensity of the lines with bias is indicative of charge state plateaus. Cross-correlation measurements demonstrate that all three lines originate from the same single QD (see section S3 of Supplement 1), and the lines are therefore attributed to different charge states of a single QD. Resonant excitation measurements with higher resolution (shown later) reveal that the line at 893 nm comprises the two fine structure split states typical of X^0, the neutral exciton [26]. In the following, we focus on the X^0 and X^- spectral lines. The X^+ spectral line shows qualitatively similar behavior to the X^0 and X^- spectral lines, but has not been investigated in detail.

In addition to demonstrating charge state selectivity, Fig. 1(d) shows that the wavelength of each spectral line is electrically tunable. A DC Stark blue shift of the QD emission of up to 0.3 meV is observed as the bias is increased. For each spectral line, the Stark-tuning range is at least five times greater than the respective spectral width. This enables tuning of the QD into and out of resonance with a narrow linewidth probe laser, a technique that is used extensively in our measurements. For applications requiring a larger QD tuning range, we note that this can be achieved either by using QDs emitting at a longer wavelength [27] or by growing AlGaAs tunneling barriers on either side of the QDs [28].

B. Electrically Tunable Resonance Fluorescence

Recent reports have demonstrated that resonant excitation enables the generation of highly coherent, indistinguishable single photons from QDs [21,29,30]. With this in mind, we first demonstrate electrically tunable RF from the X^0 and X^- spectral lines of the QD (RF was also observed from the X^+ spectral line, but

will not be discussed here). The waveguide-coupled RF was obtained by exciting the QD from above with a continuous-wave (CW) narrowband laser and collecting the scattered photons from one BGC. The RF intensity as a function of the laser wavelength and sample bias is shown in Fig. 2(a), for a laser power above the objective lens of 425 nW. RF from both the X^0 and X^- lines is observed, with a sharp transition between the two states at ~6.9 V. The transition is significantly more abrupt than for non-resonant PL with above-bandgap excitation [see Fig. 1(d)] and is a result of the elimination of background free carriers in the vicinity of the QD when using resonant excitation. We note that the *p-i-n* diode stabilizes the QD charge environment [21], which is required to observe RF. In contrast, in devices without electrical contacts, an additional non-resonant laser is typically required [3,31,32].

The high-resolution RF measurement reveals that the X^0 spectral line comprises a fine structure-split doublet. Figures 2(b) and 2(c) show RF spectra for the higher (lower) energy X_1^0 (X_2^0) fine structure states, taken from the data in Fig. 2(a). The spectra were obtained by sweeping the bias while fixing the excitation wavelength at 892.995 nm. Linewidths of 4.8 ± 0.2 μeV (1150 ± 40 MHz) and 3.1 ± 0.2 μeV (740 ± 50 MHz) are measured for X_1^0 and X_2^0, respectively. The fine structure splitting is ~36 μeV (~8.7 GHz). The contrasting intensities measured for the two states are thought to be due to the relative orientation of the orthogonal linearly polarized dipoles of the fine structure states with respect to the PhCWG, resulting in different waveguide coupling strengths (β factors) for the two states [1]. A resonant Hanbury Brown and Twiss (HBT) measurement on the X_1^0 spectral line gave a $g^{(2)}(0)$ value of 0.16 ± 0.04, showing that the QD scatters single photons [inset of Fig. 2(b)]. The non-zero value of $g^{(2)}(0)$ is due in part to the collection of PL emission from other QDs emitting at longer wavelengths than the laser, as the RF signal was not spectrally filtered. The value of $g^{(2)}(0)$ is also limited by the detector response time (700 ps). Figure 2(d) shows an RF spectrum for the X^- line at a fixed excitation wavelength of 895.85 nm. The linewidth of this transition is determined to be 5.1 ± 0.1 μeV (1240 ± 30 MHz). The apparent difference in intensity between X^- and X_1^0 is most likely an artifact due to minimizing the laser background scatter separately for the two spectral lines.

To probe the effect of the PhCWG on the recombination dynamics of the QD, a resonant lifetime measurement was undertaken on the X_1^0 spectral line using pulsed excitation. The excitation and collection geometry was the same as for the CW RF measurements. The lifetime was determined to be 442 ± 3 ps, corresponding to a transform limited linewidth of ~1.5 μeV. For comparison, a lifetime of 750 ps was measured for an ensemble of QDs situated in the bulk of the wafer. The Purcell factor is therefore estimated to be 1.7. Additionally, a coherence time of 670 ± 20 ps was measured under low power, CW resonant excitation (~40 nW) for the X_1^0 state using Michelson interferometry. In combination with the measured lifetime, this results in a long pure dephasing time of 2.8 ± 0.1 ns (see Materials and Methods). Our nano-photonic device therefore supports highly coherent QD emission, despite the proximity of

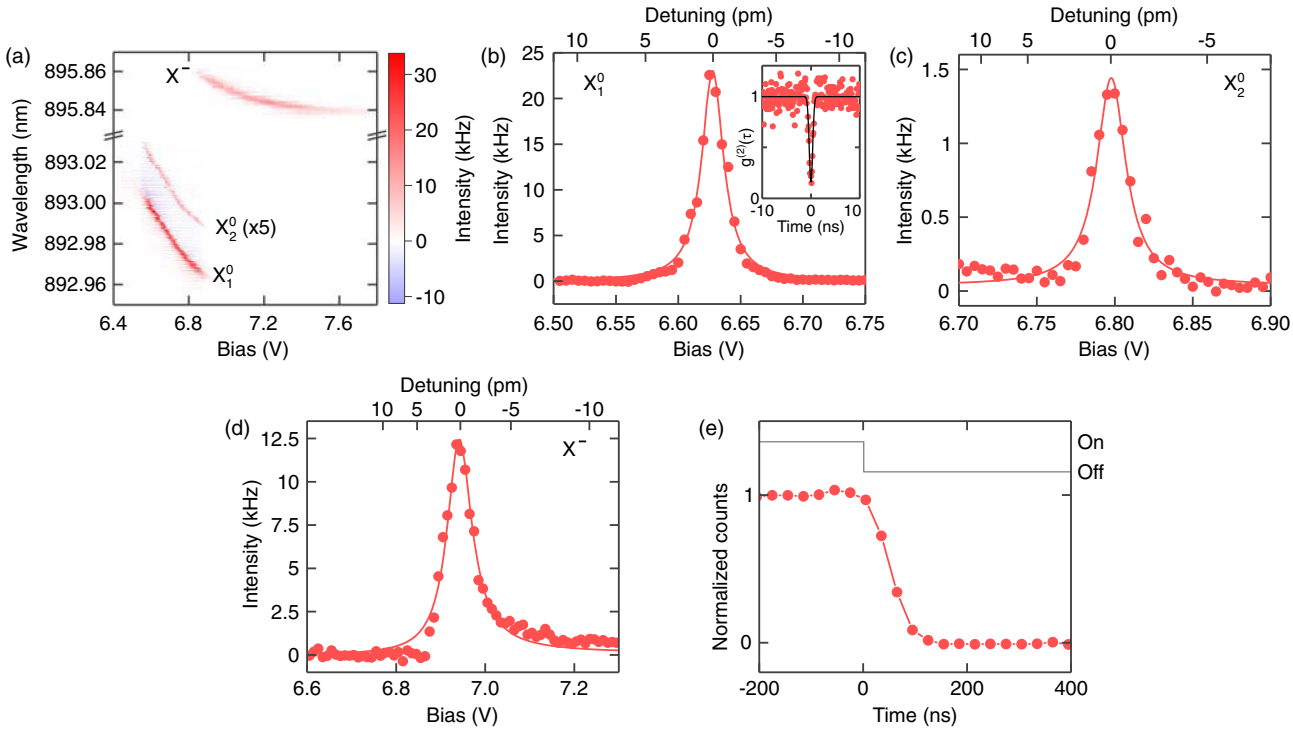

Fig. 2. Resonance fluorescence (RF) from a QD in the photonic crystal waveguide. (a) RF intensity as a function of wavelength and bias for the neutral fine structure states (X_1^0 and X_2^0) and charged state (X^-) of a single QD. The X_2^0 state intensity has been scaled by a factor of 5 for clarity. (b) and (c) Swept-bias RF spectra (circles) for the (b) higher energy X_1^0 state and (c) lower energy X_2^0 state of the neutral exciton at a fixed excitation wavelength of $\lambda = 892.995$ nm. Inset in (b) shows the second-order correlation function for photons scattered from the X_1^0 spectral line. (d) Swept-bias RF spectrum (circles) for the X^- state of the same QD at a fixed wavelength of 895.85 nm. Solid lines are Lorentzian fits to the data. (e) Electrical switching of the RF from the X_1^0 state for $\lambda = 893$ nm (circles; the lower red line is a guide for the eye). The upper gray line indicates the X_1^0-laser detuning during the measurement ("on"–resonant, "off"–non-resonant).

the QD to numerous etched surfaces. This is likely due in part to charge stabilization provided by the *p-i-n* structure, and the use of resonant excitation.

Figure 2(e) shows dynamical electrical tuning of the RF from the X_1^0 spectral line. A 10% to 90% switching time as short as 80 ns is measured. This is significantly faster than switching by modulating the weak non-resonant laser commonly used in QD RF measurements in devices lacking a diode structure [3,32]. The switching time is limited by the large area of the diode used in this work (~0.1 mm^2). Use of a micro-diode contacting scheme would reduce the RC time constant of the diode and allow GHz frequency modulation of the RF signal [20]. High-frequency electrical control can also allow the QD transition to be locked to an external laser to enable generation of frequency-stabilized single photons [33]. This structure thus presents a promising route for sourcing of highly coherent, rapidly switchable and tunable waveguide-coupled single photons for integrated quantum optical networks.

C. Waveguide Transmission Controlled by a Single Tunable Quantum Dot

The QD is a versatile nano-photonic resource. In addition to acting as a resonant scattering single-photon source, we demonstrate that it can also act as an electrically tunable optical nonlinear element at the single-photon level. The nonlinearity arises due to differing outcomes when single or multiple photons scatter from the QD within one excited state lifetime. For single-photon scattering, quantum interference leads to preferential reflection (dipole-induced reflection), thereby reducing the waveguide transmission. Conversely, preferential transmission occurs for incident states containing two photons [34]. This constitutes a nonlinear interaction at the single-photon level. To probe the nonlinear interaction, we inject a weak coherent laser into the waveguide. At sufficiently low power, the laser field predominantly comprises zero- and one-photon states, when measured in a time window equal to the QD lifetime. As single photons are reflected by the QD, extinction of the transmission is therefore measured on resonance.

Figure 3(a) shows the waveguide transmission as a function of laser wavelength and applied voltage when the laser is tuned across the X^0 and X^- states of the same QD. The transmission is normalized at each point to the transmission measured with the QD in an optically inactive state (at a bias of 5 V). The power incident on the input BGC was 8.5 nW, chosen to maximize the extinction of the laser by the QD. When the laser is resonant with the X_1^0 spectral line, a maximum laser extinction of 40 ± 2% is observed. The X_2^0 line shows a weaker interaction with the laser (extinction up to 9 ± 1%), consistent with the lower intensity seen for this spectral line in RF measurements. For the X^- state, the maximum transmission extinction is 20 ± 1%. The voltage dependence of the interaction of the laser and QD states is consistent with the RF measurements [see Fig. 2(a)], with an abrupt switch in QD charge state occurring at ~6.9 V. Figures 3(b) and 3(c) show representative transmission spectra for the X^0 and

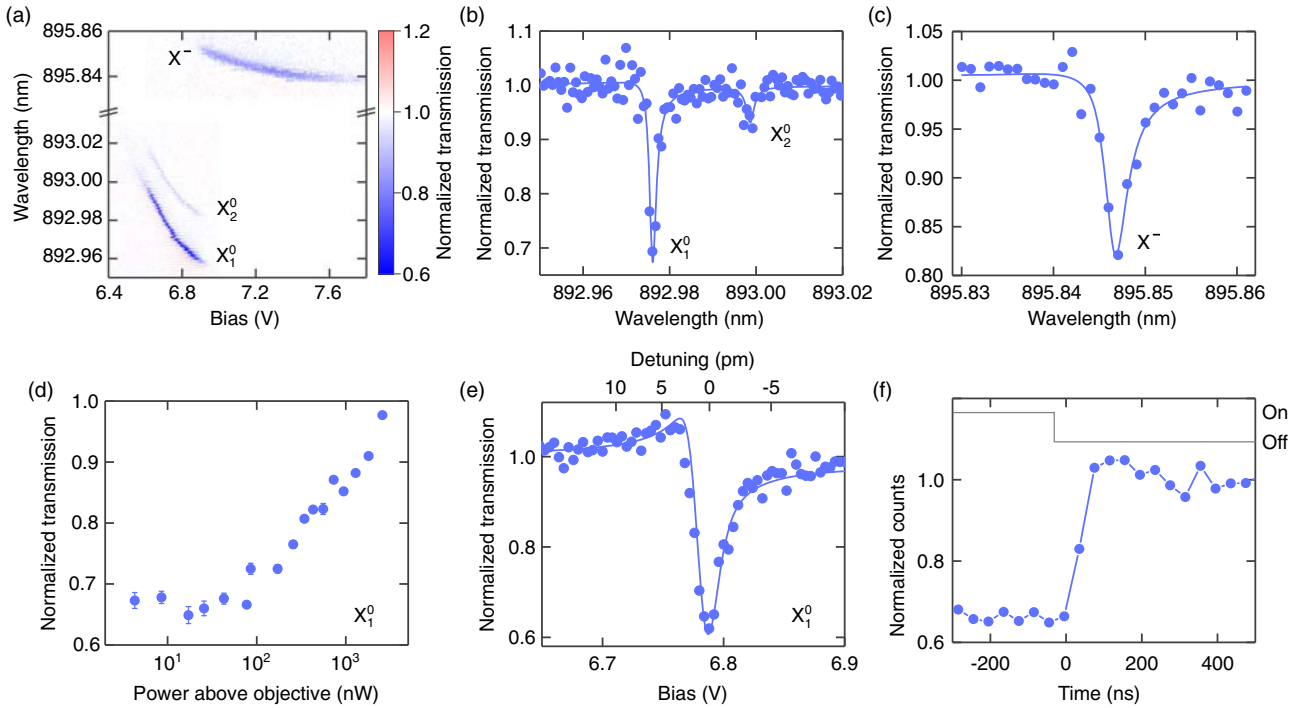

Fig. 3. Resonant transmission through the photonic crystal waveguide. (a) Normalized transmission as a function of wavelength and bias for the neutral fine structure states (X_1^0 and X_2^0) and charged state (X^-) of a single QD. (b) and (c) Normalized transmission spectra (circles) for the (b) X_1^0 and X_2^0 states of the neutral exciton at a bias of 6.73 V and (c) the X^- state of the same QD at 7.06 V. Solid lines are Breit–Wigner–Fano fits to the data. (d) Normalized transmission on resonance with the X_1^0 spectral line as a function of laser power, for $\lambda = 892.99$ nm. Error bars are derived from the fitting procedure used to determine the minimum transmission at each power. (e) Transmission extinction measured on resonance with the X_1^0 spectral line by sweeping the bias at fixed wavelength ($\lambda = 892.97$ nm). The upper abscissa gives the detuning calculated using the voltage-wavelength dependence determined from (a). The voltage sweep precludes any wavelength-dependent variation in the scattered laser suppression. The solid line shows the transmission predicted by a transfer matrix model (see main text and Supplement 1.). (f) Electrical switching of transmission by the X_1^0 spectral line (circles; the lower blue line is a guide for the eye). The upper gray line indicates the X_1^0-laser detuning during the measurement ("on"–resonant, "off"–non-resonant).

X^- spectral lines at fixed biases of 6.73 V and 7.06 V, respectively. The dispersive Fano lineshapes are due to interference between the discrete QD spectral lines and the continuum of photonic states arising from Fabry–Perot modes formed by reflection from the BGCs and photonic crystal–nanobeam interfaces [3]. Each spectrum is fitted with a Breit–Wigner–Fano function, allowing for the probability of scattering into continuum states. Linewidths of 3.7 ± 0.2 μeV (890 ± 50 MHz) for X_1^0, 3.3 ± 0.3 μeV (800 ± 70 MHz) for X_2^0, and 4.6 ± 0.5 μeV (1100 ± 100 MHz) for X^- are extracted from the fitting procedure.

As the input laser power is increased, higher photon numbers begin to dominate within the laser field, and the transmission extinction reduces accordingly, demonstrating the nonlinear nature of the interaction [see Fig. 3(d)]. The relatively high power incident on the BGC required to observe saturation of the QD implies that the in-coupling efficiency is lower than expected, on the order of 1%. This is likely due to deviation of the fabricated BGC dimensions from design.

The maximum transmission contrast of 40% reported here is significantly higher than that measured in single-pass waveguide structures without electrical control [3,6], and comparable with a coupled cavity-waveguide approach [5] but with the highly desirable property of broadband waveguide coupling. Deterministic coupling of single photons with the QD is required for many future device applications. To identify the factors that currently limit the transmission contrast, we model the device using the transfer matrix method (see Supplement 1 section S4 for full details). Figure 3(e) shows the results of the model alongside the experimental transmission as a function of the X_1^0-laser detuning. The degree of QD blinking (probability of the QD being in an "off" state) was used as the only fitting parameter in the model, with a relatively small value of 9% describing the data well. This is in agreement with the absence of any clear blinking being observed on the second timescale of the transmission measurements. From the model, we conclude that approaching the transform limit for the QD linewidth and increasing the Purcell factor to 5 would result in over 90% transmission extinction (see Supplement 1 Fig. S6). These values are achievable with current technological capabilities. The linewidth of the X_1^0 spectral line studied here is already only a factor of 2.5 greater than the transform limit, but could be improved with greater control over charge and spin noise in the vicinity of the QD [22]. A larger Purcell enhancement should be achievable in the waveguide geometry, with values up to 30 predicted theoretically for slow-light PhCWGs [24].

The extinction of the laser by the QD can be switched rapidly using electrical tuning in the same manner as the RF signal. Figure 3(f) shows the switching response of the device when the X_1^0 line is tuned out of resonance with the laser. The transmission state is switched in as little as 60 ns, in agreement with the RF switching time. This measurement demonstrates that the X_1^0 spectral line can therefore be used to switch the transmission state in the current device at a frequency of ~10 MHz. As noted above in the case of RF, optimization of the diode structure would enable GHz switching speeds [20].

D. Photon Statistics and Optical Nonlinearity

The quantum nature of the nonlinear photon–QD interaction was confirmed using photon statistics measurements on the reflected and transmitted laser fields, with the laser resonant with the X_1^0 spectral line. For measurements in the reflection geometry, the excitation and collection polarizers were aligned ~45 deg and ~135 deg to the input BGC, respectively. The effective power above the objective in this case is estimated to be ~10 nW. Figure 4(a) shows the resulting histogram of correlated events binned by time delay when detecting photons reflected by the QD. Clear antibunching at zero time delay is observed, with a minimum value of ~0.35, showing that single photons are reflected by the QD. Note that the data are uncorrected for the background laser scatter, which increases when the excitation and collection locations are overlapped for the reflection measurement (the signal-to-background ratio in this case is ~6:1).

Reflection of single photons by the QD results in the transmitted laser field consisting preferentially of two-photon components, and bunching is therefore expected in the photon statistics for the transmitted field. Furthermore, the probability of transmission of two photons has been predicted theoretically to increase due to the formation of a bound (frequency entangled) two-photon state, for which constructive (destructive) interference occurs in the direction of transmission (reflection) [34]. For photon statistics measurements in the transmission geometry, the laser power above the objective was 8.5 nW, and the transmission dip on resonance was 20% (reduced relative to Fig. 3, as

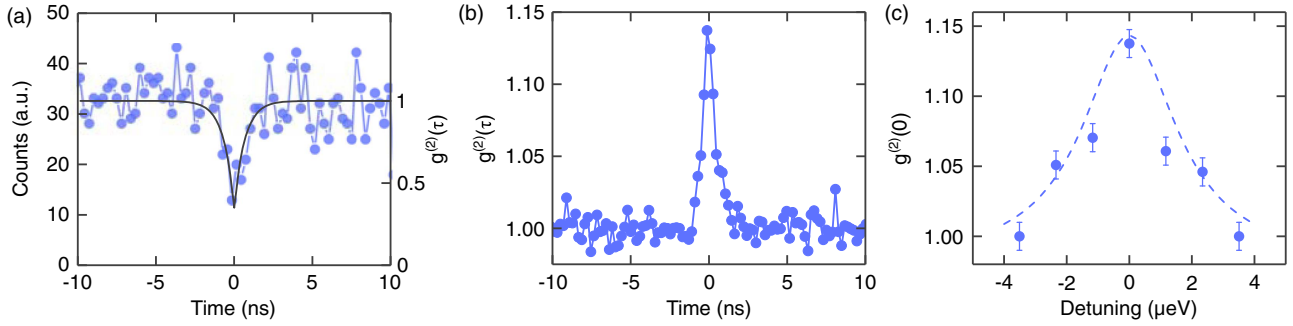

Fig. 4. Photon statistics for reflected and transmitted photons resonant with the X_1^0 spectral line. (a) Second-order autocorrelation measurement for reflected photons at zero X_1^0-laser detuning, showing antibunching at zero time delay (points). The data are not corrected for the laser background. The solid black line is a double-sided exponential fit to the data, with a minimum value corresponding to $g^{(2)}(0) \sim 0.35$. The histogram bin width is 300 ps. (b) Second-order autocorrelation measurement for transmitted photons at zero X_1^0-laser detuning. Clear bunching is observed at zero time delay. The histogram bin width is 200 ps. (c) Maximum bunching of transmitted photons versus X_1^0-laser detuning (circles). Error bars equal one standard deviation in the noise level. The dashed line is a Lorentzian with the X_1^0 transmission linewidth of 3.7 μeV as a guide to the eye.

the alignment of input and output polarizers was optimized for maximum photon detection count rate rather than transmission contrast). Figure 4(b) shows the resulting autocorrelation histogram. Clear bunching of 1.14 ± 0.01 is observed on the timescale of the X_1^0 lifetime. The degree of bunching is greater than that measured previously for a QD in a PhCWG without electrical charge stabilization [3]. Note that for higher input powers, the degree of bunching would decrease due to saturation of the QD, ultimately resulting in Poissonian statistics at high power [3].

Figure 4(c) shows the degree of bunching of transmitted photons as a function of the X_1^0-laser detuning. The detuning is controlled by fixing the laser wavelength and electrically tuning the X_1^0 transition. At large detuning values, $g^{(2)}(0)$ approaches unity, as expected for a coherent laser source described by Poissonian statistics. The value of $g^{(2)}(0)$ increases from unity as the detuning is reduced and reaches a maximum of 1.14 for zero detuning. The width of the detuning curve is close to the 3.7 μeV spectral width of the X_1^0 transition (shown as a dashed Lorentzian curve), clearly demonstrating that the degree of bunching is dependent on the strength of the interaction between the laser and the QD.

3. CONCLUSION

In conclusion, we have demonstrated electrical control of resonant scattering from a single QD embedded in a nano-photonic waveguide. The QD was shown to act both as a source of electrically tunable, waveguide-coupled single photons and as a nonlinear element to control photon–photon interactions in the waveguide. High-purity single-photon emission was demonstrated under resonant excitation with $g^{(2)}(0) = 0.16$. The transmission of a weak coherent laser through the waveguide was modulated by up to 40% by electrically controlling the QD-laser detuning. Antibunching of the reflected photons and detuning dependent bunching of the transmitted photons revealed the quantum nature of the nonlinearity.

Achieving complete transmission extinction is highly desirable, resulting in a pi phase shift being applied to every scattered single photon (see e.g., [35]). The narrow linewidths reported here for a QD embedded in a PhCWG represent very encouraging progress towards the transform-limited linewidths that complete transmission extinction requires. Electrical control of the quantum optical nonlinearity opens up several promising avenues for future research. In particular, many quantum optical devices require two or more indistinguishable emitters. This work demonstrates that the electrical approach to QD energy tuning (required to overcome spectral mismatch between QDs) is fully compatible with the realization of a single-photon nonlinearity in a waveguide-coupled geometry. Electrical tuning is a local approach [36] and will allow for individual electrical control of separate QDs coupled to the same waveguide mode. One can also envisage a realization of the quantum optical controlled-phase gate [7], containing two QDs tuned into resonance via the DC Stark effect.

4. MATERIALS AND METHODS

Optical measurements were undertaken with the sample mounted in a homemade gas exchange cryostat operating at 4.2 K. The cryostat had optical access from above the sample, which was positioned using ultrastable x, y, and z piezo stages. Independent spatial selectivity of excitation and collection locations was enabled using fiber-coupled optics external to the cryostat.

CW resonant optical measurements were performed using a narrowband, widely tunable CW Ti:Sapphire laser (SolsTiS-1000-SRX-XF-TS3, M Squared Lasers). Rejection of the scattered laser background in resonant measurements was achieved using a combination of spatial and polarization filtering. A differential technique was also employed to remove residual background laser scatter. This entailed electrically switching the QD into and out of resonance with the laser at a frequency of 1 kHz-10 kHz, and evaluating the difference signal ("resonant" minus "off resonant"). A signal-to-background ratio of up to 200:1 was obtained in the case of CW resonance fluorescence, upon exciting a QD in the PhCWG from above and collecting the resulting waveguide-coupled scattered photons from one of the BGCs.

For HBT measurements, the optical signal was split using a 50:50 fiber beam splitter and detected by two avalanche photodiodes (APDs). Correlations between detection events were analyzed using a time-correlated single-photon counting card (Becker-Hickl SPC-130). The convolved instrument response time for this measurement was 700 ps.

Resonant lifetime measurements were undertaken using a picosecond pulsed Ti:Sapphire laser (Spectra-Physics Tsunami, Newport). A monochromator was used to create a narrow bandwidth excitation pulse with a width of ~10 pm. The QD was excited from above, and scattered photons were collected from one BGC and detected on a superconducting nanowire single-photon detector with a time resolution of 50 ps (Single Quantum Eos). The SPC-130 single-photon counting card was used to correlate the arrival times of scattered photons with a reference pulse from a photodiode. To account for background scatter, the QD was electrically modulated on and off resonance with the laser. Events detected in the off-resonance case were removed from the data obtained in the resonance case, thus removing background scatter from the measurement.

To determine the QD exciton coherence time, photons scattered resonantly from the QD under CW excitation were passed through a free-space Michelson interferometer, one arm of which contained a variable delay line. The interference signal as a function of time delay between the two arms was read out using an APD. The pure dephasing time was calculated from the well-known expression $1/T_2 = 1/2T_1 + 1/T_2^*$, where T_1 and T_2 are the QD lifetime and coherence time, respectively, and T_2^* is the pure dephasing time.

Funding. Engineering and Physical Sciences Research Council (EPSRC) (EP/N031776/1).

Acknowledgment. The sample was made by B. R. and E. C. The experiments were performed by D. H. and A. P. F. The experiment was conceived and the work directed by L. R. W., M. S. S., I. E. I., and A. M. F. The theoretical model was created by D. L. H. and P. K. The paper was written by A. P. F. and D. H. with contributions from all authors. Data supporting this publication can be freely downloaded from the University of Sheffield Research Data Repository at http://dx.doi.org/10.15131/shef.data.6022811, under the terms of the Creative Commons Attribution (CC-BY) license.

See Supplement 1 for supporting content.

[†]These authors contributed equally to this work.

REFERENCES

1. M. Arcari, I. Söllner, A. Javadi, S. Lindskov Hansen, S. Mahmoodian, J. Liu, H. Thyrrestrup, E. H. Lee, J. D. Song, S. Stobbe, and P. Lodahl, "Near-unity coupling efficiency of a quantum emitter to a photonic crystal waveguide," Phys. Rev. Lett. **113**, 093603 (2014).
2. T. Lund-Hansen, S. Stobbe, B. Julsgaard, H. Thyrrestrup, T. Sünner, M. Kamp, A. Forchel, and P. Lodahl, "Experimental realization of highly efficient broadband coupling of single quantum dots to a photonic crystal waveguide," Phys. Rev. Lett. **101**, 113903 (2008).
3. A. Javadi, I. Söllner, M. Arcari, S. L. Hansen, L. Midolo, S. Mahmoodian, G. Kiršanskė, T. Pregnolato, E. H. Lee, J. D. Song, S. Stobbe, and P. Lodahl, "Single-photon non-linear optics with a quantum dot in a waveguide," Nat. Commun. **6**, 8655 (2015).
4. S. Kalliakos, Y. Brody, A. J. Bennett, D. J. P. Ellis, J. Skiba-Szymanska, I. Farrer, J. P. Griffiths, D. A. Ritchie, and A. J. Shields, "Enhanced indistinguishability of in-plane single photons by resonance fluorescence on an integrated quantum dot," Appl. Phys. Lett. **109**, 151112 (2016).
5. A. Sipahigil, R. E. Evans, D. D. Sukachev, M. J. Burek, J. Borregaard, M. K. Bhaskar, C. T. Nguyen, J. L. Pacheco, H. A. Atikian, C. Meuwly, R. M. Camacho, F. Jelezko, E. Bielejec, H. Park, M. Lončar, and M. D. Lukin, "An integrated diamond nanophotonics platform for quantum-optical networks," Science **354**, 847–850 (2016).
6. M. K. Bhaskar, D. D. Sukachev, A. Sipahigil, R. E. Evans, M. J. Burek, C. T. Nguyen, L. J. Rogers, P. Siyushev, M. H. Metsch, H. Park, F. Jelezko, M. Lončar, and M. D. Lukin, "Quantum nonlinear optics with a germanium-vacancy color center in a nanoscale diamond waveguide," Phys. Rev. Lett. **118**, 223603 (2017).
7. A. Nysteen, D. P. S. McCutcheon, M. Heuck, J. Mørk, and D. R. Englund, "Limitations of two-level emitters as nonlinearities in two-photon controlled-PHASE gates," Phys. Rev. A **95**, 062304 (2017).
8. I. Fushman, D. Englund, A. Faraon, N. Stoltz, P. Petroff, and J. Vuckovic, "Controlled phase shifts with a single quantum dot," Science **320**, 769–772 (2008).
9. H. Kim, R. Bose, T. C. Shen, G. S. Solomon, and E. Waks, "A quantum logic gate between a solid-state quantum bit and a photon," Nat. Photonics **7**, 373–377 (2013).
10. M. A. Pooley, D. J. P. Ellis, R. B. Patel, A. J. Bennett, K. H. A. Chan, I. Farrer, D. A. Ritchie, and A. J. Shields, "Controlled-NOT gate operating with single photons," Appl. Phys. Lett. **100**, 211103 (2012).
11. E. Knill, G. J. Milburn, R. Laflamme, and G. J. Milburn, "A scheme for efficient quantum computation with linear optics," Nature **409**, 46–52 (2001).
12. P. Kok, W. J. Munro, K. Nemoto, T. C. Ralph, J. P. Dowling, and G. J. Milburn, "Linear optical quantum computing with photonic qubits," Rev. Mod. Phys. **79**, 135–174 (2007).
13. D. E. Chang, V. Gritsev, G. Morigi, V. Vuletić, M. D. Lukin, and E. A. Demler, "Crystallization of strongly interacting photons in a nonlinear optical fibre," Nat. Phys. **4**, 884–889 (2008).
14. I. Shomroni, S. Rosenblum, Y. Lovsky, O. Bechler, G. Guendelman, and B. Dayan, "All-optical routing of single photons by a one-atom switch controlled by a single photon," Science **345**, 903–906 (2014).
15. D. E. Chang, A. S. Sørensen, E. A. Demler, and M. D. Lukin, "A single-photon transistor using nano-scale surface plasmons," Nat. Phys. **3**, 807–812 (2007).
16. R. B. Patel, A. J. Bennett, I. Farrer, C. A. Nicoll, D. A. Ritchie, and A. J. Shields, "Two-photon interference of the emission from electrically tunable remote quantum dots," Nat. Photonics **4**, 632–635 (2010).
17. S. G. Carter, T. M. Sweeney, M. Kim, C. S. Kim, D. Solenov, S. E. Economou, T. L. Reinecke, L. Yang, A. S. Bracker, and D. Gammon, "Quantum control of a spin qubit coupled to a photonic crystal cavity," Nat. Photonics **7**, 329–334 (2013).
18. D. Pinotsi, P. Fallahi, J. Miguel-Sanchez, and A. Imamoglu, "Resonant spectroscopy on charge tunable quantum dots in photonic crystal structures," IEEE J. Quantum Electron. **47**, 1371–1374 (2011).
19. Y. Cao, A. J. Bennett, D. J. P. Ellis, I. Farrer, D. A. Ritchie, and A. J. Shields, "Ultrafast electrical control of a resonantly driven single photon source," Appl. Phys. Lett. **105**, 051112 (2014).
20. F. Pagliano, Y. Cho, T. Xia, F. van Otten, R. Johne, and A. Fiore, "Dynamically controlling the emission of single excitons in photonic crystal cavities," Nat. Commun. **5**, 5786 (2014).
21. N. Somaschi, V. Giesz, L. De Santis, J. C. Loredo, M. P. Almeida, G. Hornecker, S. L. Portalupi, T. Grange, C. Antón, J. Demory, C. Gómez, I. Sagnes, N. D. Lanzillotti-Kimura, A. Lemaítre, A. Auffeves, A. G. White, L. Lanco, and P. Senellart, "Near-optimal single-photon sources in the solid state," Nat. Photonics **10**, 340–345 (2016).
22. A. V. Kuhlmann, J. H. Prechtel, J. Houel, A. Ludwig, D. Reuter, A. D. Wieck, and R. J. Warburton, "Transform-limited single photons from a single quantum dot," Nat. Commun. **6**, 8204 (2015).
23. S. Hughes, "Enhanced single-photon emission from quantum dots in photonic crystal waveguides and nanocavities," Opt. Lett. **29**, 2659–2661 (2004).
24. V. S. C. Manga Rao and S. Hughes, "Single quantum-dot Purcell factor and β factor in a photonic crystal waveguide," Phys. Rev. B **75**, 205437 (2007).
25. D. Pinotsi, J. M. Sanchez, P. Fallahi, A. Badolato, and A. Imamoglu, "Charge controlled self-assembled quantum dots coupled to photonic crystal nanocavities," Photon. Nanostruct. **10**, 256–262 (2012).
26. M. Bayer, G. Ortner, O. Stern, A. Kuther, A. A. Gorbunov, A. Forchel, P. Hawrylak, S. Fafard, K. Hinzer, T. L. Reinecke, S. N. Walck, J. P. Reithmaier, F. Klopf, and F. Schäfer, "Fine structure of neutral and charged excitons in self-assembled In(Ga)As/(Al)GaAs quantum dots," Phys. Rev. B **65**, 195315 (2002).
27. A. Laucht, F. Hofbauer, N. Hauke, J. Angele, S. Stobbe, M. Kaniber, G. Böhm, P. Lodahl, M. C. Amann, and J. J. Finley, "Electrical control of spontaneous emission and strong coupling for a single quantum dot," New J. Phys. **11**, 23034 (2009).
28. A. J. Bennett, R. B. Patel, J. Skiba-Szymanska, C. A. Nicoll, I. Farrer, D. A. Ritchie, and A. J. Shields, "Giant Stark effect in the emission of single semiconductor quantum dots," Appl. Phys. Lett. **97**, 031104 (2010).
29. S. Ates, S. M. Ulrich, S. Reitzenstein, A. Löffler, A. Forchel, and P. Michler, "Post-selected indistinguishable photons from the resonance fluorescence of a single quantum dot in a microcavity," Phys. Rev. Lett. **103**, 167402 (2009).
30. Y.-M. He, Y. He, Y.-J. Wei, D. Wu, M. Atatüre, C. Schneider, S. Höfling, M. Kamp, C.-Y. Lu, and J.-W. Pan, "On-demand semiconductor single-photon source with near-unity indistinguishability," Nat. Nanotechnol. **8**, 213–217 (2013).
31. M. N. Makhonin, J. E. Dixon, R. J. Coles, B. Royall, I. J. Luxmoore, E. Clarke, M. Hugues, M. S. Skolnick, and A. M. Fox, "Waveguide coupled resonance fluorescence from on-chip quantum emitter," Nano Lett. **14**, 6997–7002 (2014).
32. H. S. Nguyen, G. Sallen, C. Voisin, P. Roussignol, C. Diederichs, and G. Cassabois, "Optically gated resonant emission of single quantum dots," Phys. Rev. Lett. **108**, 057401 (2012).
33. J. H. Prechtel, A. V. Kuhlmann, J. Houel, L. Greuter, A. Ludwig, D. Reuter, A. D. Wieck, and R. J. Warburton, "Frequency-stabilized source of single photons from a solid-state qubit," Phys. Rev. X **3**, 041006 (2014).
34. H. Zheng, D. J. Gauthier, and H. U. Baranger, "Waveguide QED: many-body bound-state effects in coherent and Fock-state scattering from a two-level system," Phys. Rev. A **82**, 063816 (2010).
35. S. Fan, Ş. E. Kocabaş, and J. T. Shen, "Input-output formalism for few-photon transport in one-dimensional nanophotonic waveguides coupled to a qubit," Phys. Rev. A **82**, 063821 (2010).
36. C. Bentham, D. Hallett, N. Prtljaga, B. Royall, D. Vaitiekus, R. J. Coles, E. Clarke, A. M. Fox, M. S. Skolnick, I. E. Itskevich, and L. R. Wilson, "Single-photon electroluminescence for on-chip quantum networks," Appl. Phys. Lett. **109**, 161101 (2016).